Proceedings of ASME Turbo Expo 2019
Turbomachinery Technical Conference and Exposition
GT2019
June 17-21, 2019, Phoenix, Arizona, USA

GT2019-91632

NON-DIMENSIONAL PARAMETERS FOR COMPARING CONVENTIONAL AND COUNTER-ROTATING TURBOMACHINES

J.J. Waldren, C.J. Clark, S.D. Grimshaw, G. Pullan
Whittle Laboratory
University of Cambridge
1 JJ Thomson Avenue
Cambridge, CB3 0DY, UK
Email: jw862@cam.ac.uk

ABSTRACT

Counter-rotating turbomachines have the potential to be high efficiency, high power density devices. Comparisons between conventional and counter-rotating turbomachines in the literature make multiple and often contradicting conclusions about their relative performance. By adopting appropriate non-dimensional parameters, based on relative blade speed, the design space of conventional machines can be extended to include those with counter-rotation. This allows engineers familiar with conventional turbomachinery to transfer their experience to counter-rotating machines. By matching appropriate non-dimensional parameters the loss mechanisms directly affected by counter-rotation can be determined.

A series of computational studies are performed to investigate the relative performance of conventional and counter-rotating turbines with the same non-dimensional design parameters. Each study targets a specific loss source, highlighting which phenomena are directly due to counter-rotation and which are solely due to blade design. The studies range from two-dimensional blade sections to three-dimensional finite radius stages. It is shown that, at hub-to-tip ratios approaching unity, with matched non-dimensional design parameters, the stage efficiency and work output are identical for both types of machine. However, a counter-rotating turbine in the study is shown to have an efficiency advantage over a conventional machine of up to 0.35 percentage points for a hub-to-tip ratio of 0.65. This is due to differences in absolute velocity producing different spanwise blade designs.

INTRODUCTION

Counter-rotating turbomachines have been studied since the 1940s [1] and researchers have claimed improvements in efficiency of as much as 4% compared to conventional designs [2], as well as the potential to double the work capacity per unit engine length [3]. Despite this, counter-rotating turbines and compressors are rarely used. The published literature is often contradictory and methods for comparing counter-rotating and conventional designs vary from study to study. The first aim of this paper is to show that, by using the correct non-dimensional parameters, counter-rotating and conventional turbomachines are both elements of the same design space. Extending the conventional design space grants those familiar with conventional machines insight into the design of counter-rotating machines. The second aim is to explain the aerodynamic benefits and challenges of counter-rotating turbines and compressors in comparison with equivalent conventional rotation machines.

Applications for Counter-Rotating Machines

Counter-rotating turbines (CRTs) are being considered for use in hypersonic transport applications due to their high power-to-weight ratio. The Synergetic Air-Breathing Rocket Engine (SABRE), under development by Reaction Engines Limited (REL), is designed to provide a reusable powerplant for hypersonic aircraft and space flight. In this engine, a CRT could drive a twin-shaft air compressor [4]. A proof of concept CRT numerical design and optimisation is described by Paniagua *et al*. [5]. The benefit of a CRT in this application is primarily its reduced size and weight compared to a conventional, or normally rotating, turbine (NRT). Another application where high power density is important is the turbopump used in rocket engines. CRTs can be used to drive the liquid oxygen fuel pumps, and here, counter-rotation is claimed to reduce the size and mass of the turbine as well as being more stable at off-design conditions [6, 7].

CRTs have also been proposed for use in aero-engines designed for civil passenger aircraft where they would power counter-rotating turbofans [8], propfans [9] or open rotor devices [10,11]. Coupling the

Copyright © 2019 by ASME

counter-rotating propulsors with a CRT is attractive as it reduces the need for a gearbox as well as reducing the size and weight of the engine. There is also the option of using a counter-rotating compressor with a CRT in an aero-engine to further reduce the size and weight.

A renewable energy system incorporating CRTs is proposed by Murakami and Kanemoto [12, 13]. Wind turbine power output is smoothed by pumping water up to a storage tank when surplus power is available and then driving a turbine with the water when there is a wind power shortage. In this hybrid-power concept the same counter-rotating machine is used to both pump the water and to work as a turbine, with the water changing direction through the machine when the mode of operation changes. Counter-rotation was chosen to alleviate gearbox and torque constraints in the system.

Previous Studies Comparing Counter-Rotating and Conventional Turbomachines

Since the study by Wintucky *et al*. [2] in the 1950s, researchers have faced two key questions when comparing counter-rotation with conventional machines. First, how should counter-rotating "stages" be defined so that they can be compared with conventional stages? Secondly, which non-dimensional parameters should be fixed when comparing the two types of machines, or for comparing different counter-rotating designs, e.g. with different ratios of blade speed? Various studies have addressed these issues, either implicitly or explicitly, in a number of ways and there is currently no agreed approach. This has led to varying design methodologies [5, 8, 10, 14] which result in different conclusions about the use of counter-rotation.

When Wintucky *et al*. [2] compared CRTs and NRTs, they considered a stage to be defined by a rotor, regardless of whether it was preceded by a stator, an inlet guide vane or with no blade row upstream. It is concluded that CRTs, given similar operating conditions to NRTs, would have a 2%-4% increase in efficiency [2]. In this study, vaneless CRTs have half the number of blade rows as NRTs and this resulted in the $1 + 0.5 * N$ notation for CRTs adopted by some researchers [14–16], where N represents the number of rotors and $1+$ represents an inlet guide vane. Another interpretation of Wintucky *et al*., used by Paniagua [5, 6], is that each counter-rotating rotor has a "phantom" upstream vane with no turning. In general, work which follows the approach of Wintucky *et al*. results in claims of improved efficiency. These efficiency benefits are attributed to the reduction in number of blade rows.

Louis [17] extends the approach of Wintucky *et al*. [2] to consider the performance of CRTs with and without inlet guide vanes. The number of blade rows is used as the basis for comparison between CRTs and NRTs and the study claims that CRTs have an improvement in both efficiency and work output. Cai *et al*. [3] also use the number of rows for comparison of CRTs and NRTs, but study the type of turbine blading, i.e. impulse, reaction or axial inlet. They conclude that CRTs can achieve twice the power output per engine length with no efficiency penalty.

Both Louis [17] and Cai *et al*. [3] use the largest absolute blade speed in the denominator for the definitions of flow coefficient and stage loading coefficient, and this approach is adopted throughout the published literature. This paper will show that flow coefficients and stage loading coefficients formed using the absolute blade speed should not be used to set equivalent operating conditions for CRTs and NRTs, and are not suitable for comparing performance. By utilising the proposed relative parameters, it will be shown that previous studies achieve efficiency gains by moving across the Smith Chart, thus providing a more complete explanation of previously reported improvements.

Research into counter-rotation has also been carried out on compressors and the advantages reported include increased pressure rise and improved stall characteristics [18]. A major area of counter-rotating compressor (CRC) research has been on the speed ratio of the two rotor blades and the effect this has on stall margin [19, 20]. This seems to have moved the focus away from the definition and comparison of a stage or appropriate selection of the non-dimensional parameters. Kerrebrock *et al*. [21] were successful in designing and testing an aspirated, counter-rotating fan and were motivated by CRC's potential for light weight, high efficiency turbomachines. Kerrebrock *et al*. consider a change in reference frame when examining velocity triangles for stall margin calculations, and Sharma *et al*. [18] note the difficulty of choosing the correct reference frame when defining Reynolds numbers. However, neither Kerrebrock *et al*. [21] nor Sharma *et al*. [18] provide an approach which incorporates the frame of reference, or that can study its implications.

Approach and Layout of Paper

This paper aims to provide an intuitive framework which can be used to make comparisons of aerodynamically similar counter-rotating and conventional turbomachines. The approach taken is to build up the model fidelity step-by-step, starting with consideration of the non-dimensional design parameters, then by performing two-dimensional computational fluid dynamics (CFD) calculations, and finally through three-dimensional CFD simulations at infinite and finite radius. The expression,

$$Loss_{Total} \equiv Loss_{Profile} + Loss_{Secondary flows} + Loss_{Tip} + Loss_{Radial} + \dots \quad , \quad (1)$$

describes the decomposition of total loss into a series of contributing factors. By utilising a step-by-step modelling approach, the effect of each loss source can be isolated, identifying which are directly effected by counter-rotation, simplifying the comparison of loss sources between conventional and counter-rotating machines.

The paper is organised into five sections. First, the blade velocities and relative frames of reference of CRTs and NRTs are considered and *relative parameters* are introduced to provide a consistent means of comparison. The two-dimensional turbine model reported by Louis [17] is used to generate Smith Charts based on the new relative parameters, showing that the performance of CRTs and NRTs are identical in this case. This example is used to explain why previous studies have reported efficiency benefits from CRTs compared to NRTs. The second section uses CFD to simulate a family of two-dimensional blade sections, which are used to produce Smith Charts for CRTs and NRTs based on relative parameters. In the third section, the CFD model is extended to a three-dimensional set up that emulates a linear cascade, i.e. "infinite" radius, with finite blade span. Tip gaps and rotating endwalls are also included so that loss sources relating to tip clearance flows, endwall losses and secondary flows can be compared for matched CRT and NRT cases.

Copyright © 2019 by ASME

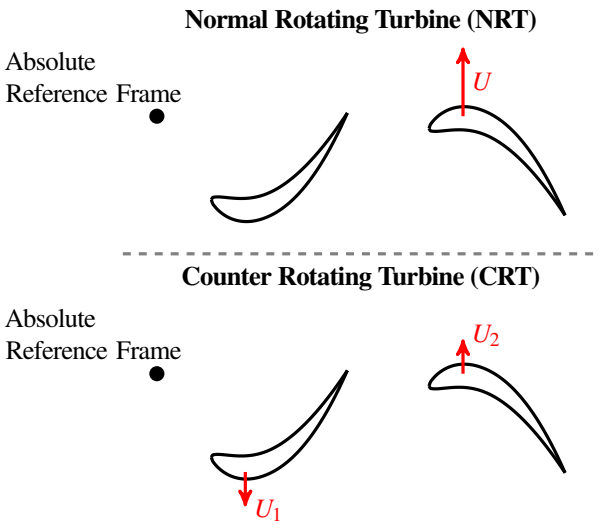

(a) Blade velocities in an absolute reference frame.

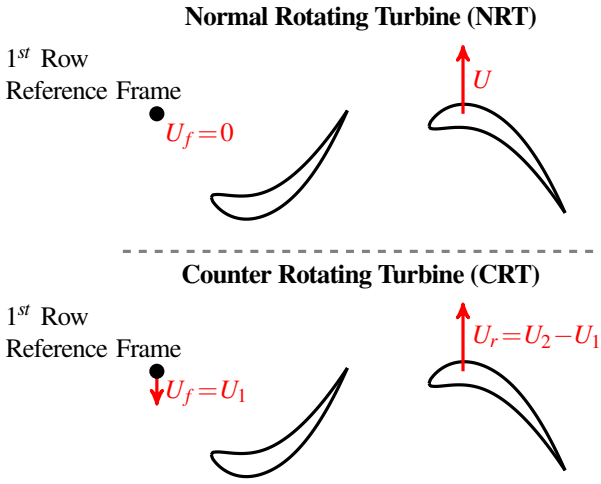

(b) Blade velocities in a reference frame relative to the first blade row.

FIGURE 1: Comparison of blade velocities for NRTs and CRTs in different reference frames.

The fourth section introduces a finite radius, finite span CFD model and this is used to study the effects of radial equilibrium. Finally, findings from the turbine study are used to compare a CRC and conventional, or normally rotating, compressor (NRC) design.

NON-DIMENSIONAL PARAMETERS

Conventional turbomachines consist of alternating blade rows of stators and rotors, with all rotor rows moving in the same direction. Counter-rotating turbomachines have adjacent rotors turning in different directions. Inter-rotor stators are not obligatory for counter-rotating turbomachines, so in this paper CRTs and CRCs will not include stators. This makes it challenging to compare conventional and counter-rotating turbomachines because it is no longer clear what is meant by a stage in a machine without stators.

Figure 1(a) shows two rows of turbine blades and their respective velocities, U, for a normal and counter-rotating turbine in an absolute frame of reference. Whilst the two turbine stages are geometrically similar, their absolute blade velocities differ and they have different conventional flow parameters ϕ and ψ. However, if the reference frame is adjusted to rotate with the first blade row at frame velocity U_f, Fig. 1(b), the turbines appear the same, both geometrically and in terms of blade velocities and velocity triangles. With this reference frame, the first CRT blade row is stationary whilst the second blade row rotates at a relative blade velocity, U_r. These two blades now look like a stage in conventional turbomachinery, and this is how a stage will be defined for counter-rotation throughout this paper. The NRT is unaffected by the change in reference frame, and is a particular solution where $U_f = 0$.

The change of reference frame is quantified by creating a new set of non-dimensional parameters, called the *relative parameters*. These are based on traditional parameters; the flow coefficient, stage loading coefficient and reaction, but defined within the relative frame. Within the reference frame, these values define the velocity triangles, hence the required blade geometries. Quantities have subscript r when defined in the rotating reference frame, and *rel* when defined relative to the second rotor. The relative flow coefficient, ϕ_r, is the ratio of axial flow velocity to the relative blade speed,

$$\phi_r = \frac{V_x}{U_r}. \tag{2}$$

The reaction, Λ, is defined using static enthalpy so it is unaffected by changing reference frame, but can be expressed as a function of relative parameters, given a constant axial velocity, which is assumed throughout the analysis.

$$\Lambda = \frac{\Delta h_{2^{nd}\text{ blade row}}}{\Delta h_{\text{Blade row pair}}} = \frac{\Delta h_{\text{'rotor'}}}{\Delta h_{\text{'stage'}}} = \frac{\psi_r + \frac{1}{2}\phi_r\left(\tan^2\alpha_{3_r} - \tan^2\alpha_{2_r}\right)}{\psi_r + \frac{1}{2}\phi_r\left(\tan^2\alpha_{3_r} - \tan^2\alpha_{1_r}\right)}. \tag{3}$$

Within the reference frame, a relative stage loading coefficient, ψ_r, is formed that is analogous to the conventional stage loading and fixes the velocity triangles.

$$\psi_r = \frac{\Delta h_{0_r}}{U_r^2} \tag{4}$$

The change of stagnation enthalpy in a reference frame rotating with the first blade row is not the same as in the absolute frame if there is net turning through the stage. This is because the reference frame itself is rotating and therefore does work,

$$\Delta h_0 = \Delta h_{0_r} + U_f\left(V_{\theta 1} - V_{\theta 3}\right). \tag{5}$$

In order to match the relative flow fields, the relative stage loading coefficient is defined in terms of the change in relative stagnation enthalpy. It can be adjusted for absolute change in stagnation enthalpy using a function of the blade speed ratio, inlet and exit relative flow angles,

$$\psi_r = \frac{\Delta h_{0_r}}{U_r^2} = \frac{\Delta h_0}{U_r^2} + \phi_r\left(\tan\alpha_{3_r} - \tan\alpha_{1_r}\right)\left(1 - \frac{U_2}{U_1}\right)^{-1} \tag{6}$$

The blade velocities can be related to the frame velocity and relative blade velocity through the expression,

$$\frac{U_f}{U_r} = \left(\frac{U_2}{U_1} - 1\right)^{-1} = \frac{U_1}{U_2 - U_1} \tag{7}$$

where rotation is considered positive in the direction of U_r. For an

Copyright © 2019 by ASME

NRT, the absolute and relative blade speeds are equal, so the new relative parameters and the traditional parameters are equivalent.

A special case occurs when modelling a repeating stage: the stage inlet and exit angles are the same, hence the change in stagnation enthalpy of the absolute and relative frames are equal, and the net work output and velocity triangles become independent of the blade velocity ratio and reference frame velocity. In this case, the blade velocity ratio solely controls the work split between the blade rows,

$$\frac{\psi_{r,1}}{\psi_{r,2}} = \frac{-U_1}{U_2}, \tag{8}$$

where the subscripts 1 and 2 represent the quantities for the first and second blade in the stage. Using a repeating stage model also enables the evaluation of relative flow angles using meanline analysis and ϕ_r, ψ_r and Λ:

$$\psi_r = 2\left(1-\Lambda-\phi_r \tan\alpha_{1_r}\right), \tag{9}$$

$$\Lambda = 1-\frac{{\phi_r}^2}{2\psi_r}\left(\tan^2\alpha_{2_r}-\tan^2\alpha_{1_r}\right). \tag{10}$$

Using Eqs. (9) and (10) with the exit Mach number relative to the second blade row and relative inlet conditions results in the relative blade speed,

$${U_r}^2 = \frac{\gamma R {M_{3_{rel}}}^2 T_{01_r}}{{\phi_r}^2\sec^2\alpha_{2_r} + \frac{\gamma R {M_{3_{rel}}}^2}{2c_p}\left(2\psi_r + {\phi_r}^2\sec^2\alpha_{1_r}\right)}. \tag{11}$$

If not using a repeating stage, an additional relative or absolute flow angle must be specified, with more involved expressions to calculate the remaining flow angles and blade speed ratio.

Equations (2) to (11) are valid for both NRTs and CRTs. Therefore, if a CRT and NRT have the same relative parameters, relative inlet conditions and relative exit Mach number, the blade geometry and relative flow field, hence mean line performance, will be the same. In addition, design techniques for NRTs can be applied to CRTs using relative parameters. Compressors also operate with this velocity triangle theory so the same analysis can be performed and will result in the same non-dimensional parameters.

In order to validate relative parameters, they are applied to the analysis of a previous study. The work by Louis [17] generated Smith Charts for NRTs and CRTs. Smith Charts are a widely used tool that provide an understanding of performance over the design space [22,23]; they are especially useful for preliminary design. Louis' study used a two-dimensional empirical loss model, analysed with traditional flow coefficient and stage loading definitions, i.e. with absolute blade speed, U. In Louis' work, the Smith Charts are constructed assuming a repeating stage, so the same approach is adopted here.

Smith Charts generated by Louis [17], using conventional non-dimensional parameters, are replotted for NRTs and CRTs with 50% reaction in Figs. 2(a) and 2(b). Figure 2(c) then shows the CRT Smith Chart plotted with relative parameters. Louis keeps the traditional non-dimensional parameters fixed when comparing CRTs and NRTs. This means that for a given point in the Smith Chart the CRT has half the relative flow coefficient and quarter the relative stage loading of the NRT (Louis defines a CRT stage as two rows). Comparing Figs. 2(a) and 2(b) leads to the conclusion that a CRT at the same point on the Smith Chart point has improved efficiency. However,

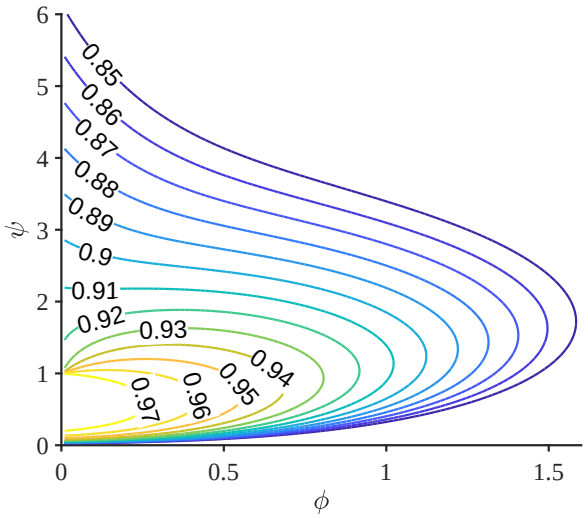

(a) NRT Smith Chart.

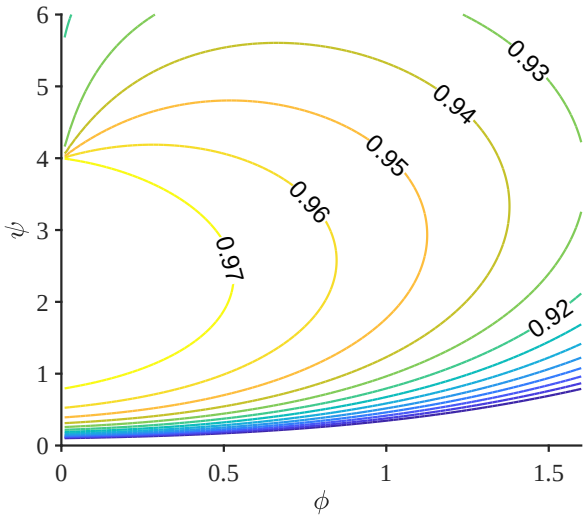

(b) CRT Smith Chart based on traditional non-dimensional parameters.

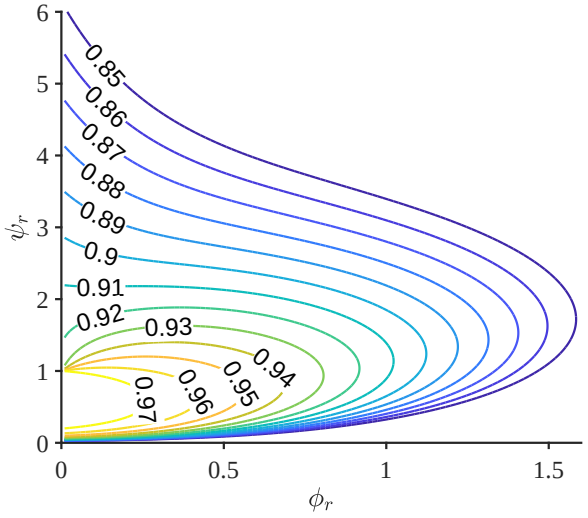

(c) CRT Smith Chart based on relative parameters.

FIGURE 2: Smith Charts showing contours of isentropic efficiency created using the method of Louis [17] comparing NRTs and CRTs using traditional non-dimensional parameters and relative parameters.

Copyright © 2019 by ASME

Fig. 2(c) reveals that the NRTs and CRTs have the same performance when compared with matched relative parameters, and the previous advantages were achieved through movement across the Smith Chart based on relative parameters. This result explains why many previous studies conclude that CRTs have higher efficiency than NRTs: analysing both types of machine with traditional non-dimensional parameters, based on absolute blade speeds, moves the operating point of CRTs to a different point on the Smith Chart defined with relative parameters. This transform, reducing both ϕ_r and ψ_r, is particularly "beneficial" in stages with high loading and flow coefficient.

In this analysis, the relative blade speed, U_r, relative exit Mach number, $M_{3_{rel}}$, and midspan radius were kept constant when comparing NRTs and CRTs. Therefore, the CRT rotors have half the absolute speed of the NRT rotors, meaning the CRT can be considered to act as an "aerodynamic gearbox". If, instead, the CRT rotors have the same absolute angular velocity as the NRT rotors and the relative parameters are matched, two potentially beneficial designs can be made. Firstly, if the CRT and NRT have the same midspan radius, each CRT blade would have the same absolute blade speed as the NRT rotor, meaning the CRT would have four times the power output per stage. The consequence of this is doubled relative Mach numbers, which can produce blade design complications [15]. Alternatively, the CRT midspan radius could be halved, resulting in the same relative blade speed for the CRT and NRT. This means the two stages would have the same midspan performance, but the CRT would have a higher power density due to the reduced radius. These possible designs are shown in Table 1.

	$\frac{U}{U_{NRT}}$	$\frac{U_r}{U_{rNRT}}$	$\frac{\Omega}{\Omega_{NRT}}$	$\frac{r_m}{r_{mNRT}}$	$\frac{M_{3_{rel}}}{M_{3_{rel\,NRT}}}$	$\frac{\Delta h_0}{\Delta h_{0NRT}}$	$\frac{\eta}{\eta_{NRT}}$
NRT	1	1	1	1	1	1	1
CRT 1	1	2	1	1	2	4	1*
CRT 2	0.5	1	0.5	1	1	1	1
CRT 3	0.5	1	1	0.5	1	1	1

* Neglecting Mach and Reynolds number effects.

TABLE 1: Comparison of CRT designs relative to an NRT with matched relative parameters.

TWO-DIMENSIONAL BLADE SECTION

Design of Numerical Study

A two-dimensional numerical study is used to investigate how profile loss varies between NRTs and CRTs. The meanline analysis does not consider any loss sources, and Fig. 2 uses an empirical model defined by Louis [17], so it is important to further validate the two-dimensional conclusions with CFD.

The blade profiles used in these calculations are generated by an in-house code known to produce acceptable designs over a wide operating range [24]. The camber-line slope increases linearly from the inlet metal angle to the outlet metal angle. The thickness distribution is defined by a power law based on the location of maximum thickness, blade stagger angle and a profile shape power

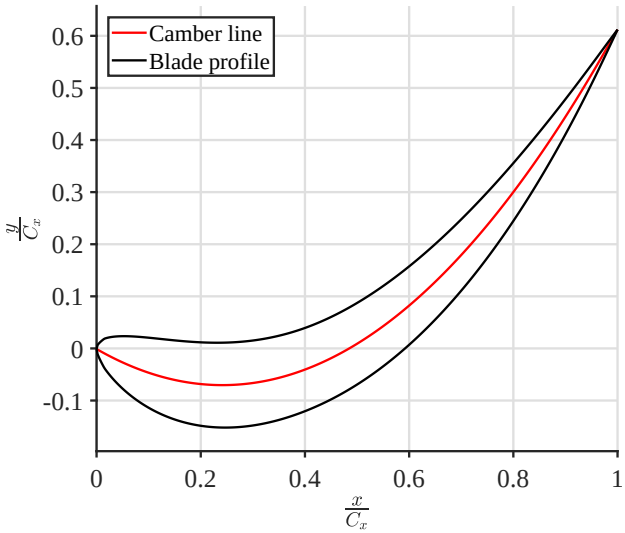

(a) Typical blade profile and camber line.

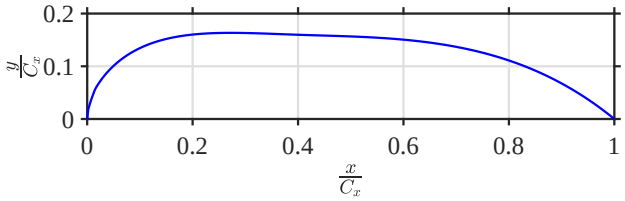

(b) Blade thickness distribution.

FIGURE 3: Graphical example of typical blade profile, with inlet metal angle of $-30°$ and outlet metal angle of $60°$.

which, in this case, is set to 3. The blades have a prescribed leading edge thickness of 10% of the maximum thickness, and zero trailing edge thickness. The metal angles used are the relative flow angles from Eqs. (9) and (10), corrected for deviation, typically around $1°$, depending on the loading. An example blade can be seen in Fig. 3.

CFD calculations were performed using Turbostream [25], with details provided in the Appendix. 81 different sets of ϕ_r and ψ_r were used for each type of turbine in the range $\phi_r = 0.4 - 1.2$ and $\psi_r = 0.75 - 2.5$. Due to an interest in multi-stage machines, a repeating stage was used in all CFD calculations. In order to keep the axial velocity close to constant and maintain a repeating stage condition, a low exit relative Mach number was chosen, $M_{3_{rel}} = 0.2$. All stages have 50% reaction and the CRT stages have equal and opposite blade velocities. As noted before, for a repeating stage, the blade velocity ratio is independent of the CRT velocity triangles. The pitch to chord ratio was calculated using a Zweifel coefficient of 0.8. The domain of each calculation includes two blade rows, with a mixing plane between the rows, and with repeating stage inlet conditions.

Results

Smith Charts from the CFD simulations are shown in Fig. 4. There is very little difference between CRT and NRT over the entire design space. This result agrees with Fig. 2; for the two-dimensional sections, CRTs and NRTs with the same relative parameters lie on the same point on a Smith Chart. Therefore, the blades are geometrically and aerodynamically identical in a reference frame rotating with the first blade row.

Copyright © 2019 by ASME

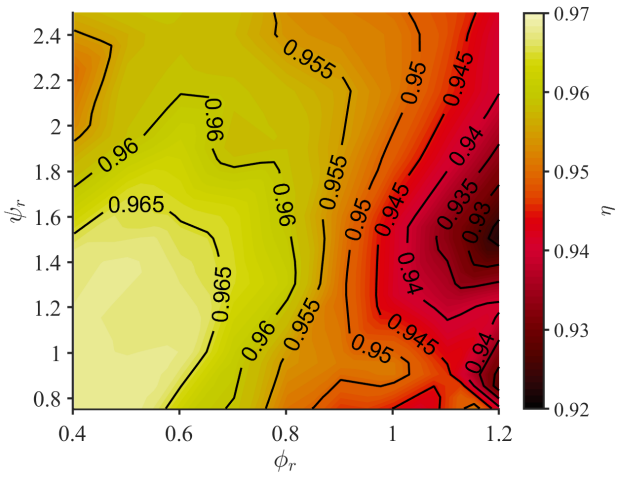

(a) NRT Smith Chart.

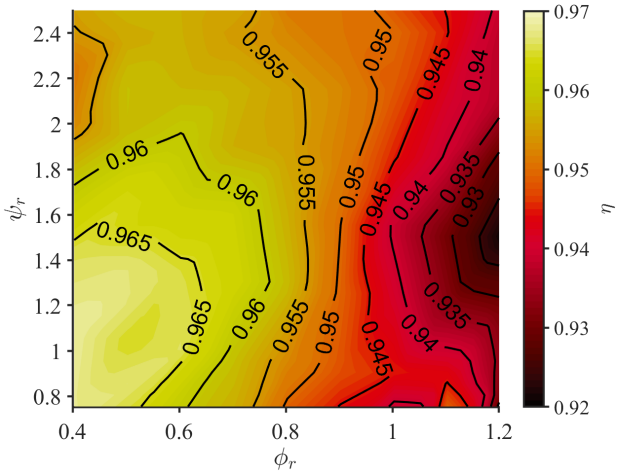

(b) CRT Smith Chart.

FIGURE 4: Smith Charts showing contours of isentropic efficiency, η, over a range of ϕ_r and ψ_r at 50% reaction. The models are two-dimensional sections run as a repeating stage.

INFINITE RADIUS, FINITE SPAN

Design of Numerical Study

Having confirmed that using relative parameters results in the same performance for NRTs and CRTs with a two-dimensional calculation, the investigation is extended to a pseudo infinite radius, three-dimensional model with a hub-to-tip radius of near unity (0.998), i.e. the simulation emulates a linear cascade. The extension to three-dimensions introduces new loss sources from endwalls and secondary flows.

In order to reduce the computational time, only one pair of relative parameters, representative of a typical highly loaded turbine, was chosen to model a two blade repeating stage. The design point and resulting blade geometries are given in Table 2. Because the hub-to-tip ratio is near unity, the blades are prismatic. In order to keep the axial velocity constant, and maintain a repeating stage condition, the annulus height increases through the stage, Fig. 5.

Three different numerical studies were carried out using the infinite radius, finite span model. First, an investigation into the effect of secondary flows and endwall losses at a fixed exit relative Mach number of $M_{3_{rel}} = 0.4$ was performed. Second, an investigation of the effect of Mach number was undertaken. During these calculations, the endwalls rotate with the adjacent blade. This means the behaviour of the endwalls is the same for CRTs and NRTs when viewed in a reference frame rotating with the first blade row.

ϕ_r	0.7	χ_1	$-35.4°$
ψ_r	2.0	χ_2	$66.0°$
Λ	50%	δ	$1.0°$
Z	0.8	Re_x	3×10^5
AR	2	$M_{3_{rel}}$	0.4

TABLE 2: Midspan design point data for the turbine study.

Finally, with an exit relative Mach number of 0.4, tip gaps of 5% span were added to the model. A CRT will likely have one blade row rotating with the hub and one cantilevered from the casing, rotating in the opposite direction. Therefore, the first blade row has a gap between the blade and the hub, whilst the second row has a gap between the blade and the casing. The casing endwall rotates with the first blade row, and the hub endwall rotates with the second blade throughout the entire domain. The same tip gaps and rotations are applied to the NRT so, when viewed in a reference frame rotating with the first blade row, the motion of the endwalls relative to the blades are the same for CRT and NRT, making an aerodynamically consistent comparison.

Results

Figure 5 shows that local pitchwise-averaged relative flow coefficients for the NRT and CRT cases, with no tip gaps and $M_{3_{rel}} = 0.4$, are nearly identical. The addition of endwall losses and secondary flows have the same effect for the NRT and CRT, resulting in the negligible difference in stage isentropic efficiency of 0.04%.

The matched performance of CRTs and NRTs is confirmed when the exit relative Mach number is varied, Fig. 6. Over the entire range, the difference in performance is never more than 0.1%. The gradual increase in efficiency with Mach number is due to increasing Reynolds number, and the sudden drop at a relative Mach number of 0.8 is due to the onset of shock losses.

The results from the third numerical study also show that NRTs and CRTs perform the same with tip gaps with a difference in isentropic efficiency of 0.04%. The local entropic loss coefficient,

$$\zeta_s = \frac{T_{0\,\text{outlet}}\left(s_{\text{outlet}} - s_{\text{inlet}}\right)}{c_p\left(T_{0\,\text{outlet}} - T_{\text{outlet}}\right)}, \tag{12}$$

is plotted at blade exit in Fig. 7. These plots show that the losses associated with tip gaps do not change when the turbine is counter-rotating.

Copyright © 2019 by ASME

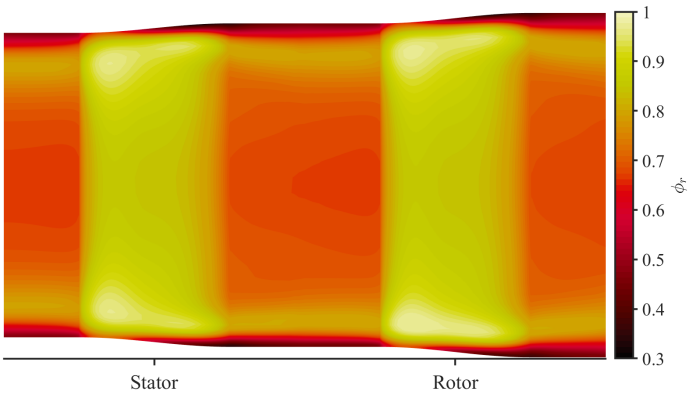

(a) NRT.

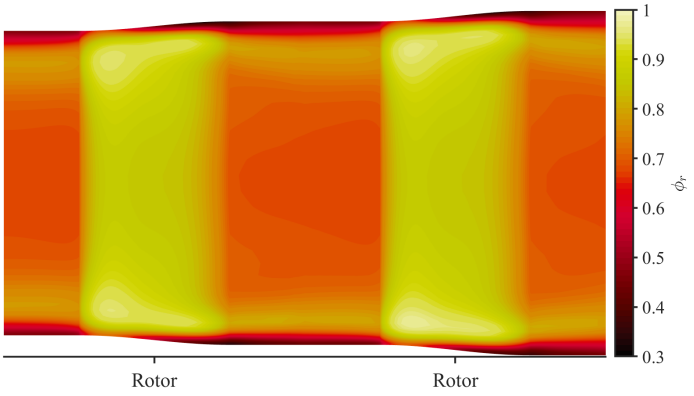

(b) CRT.

FIGURE 5: Pitchwise averaged local relative flow coefficient (ϕ_r) for NRT and CRT with no tip gaps and $M_{3_{rel}} = 0.4$. Shown in the axial-radial plane.

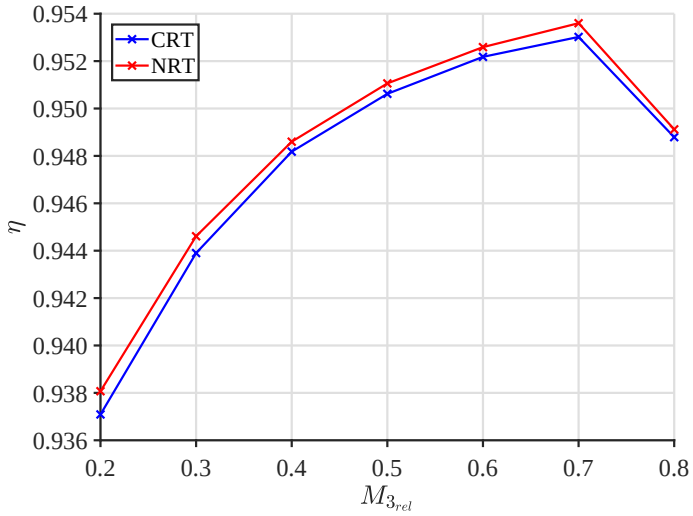

FIGURE 6: Variation of isentropic efficiency with exit relative Mach number for CRT and NRT.

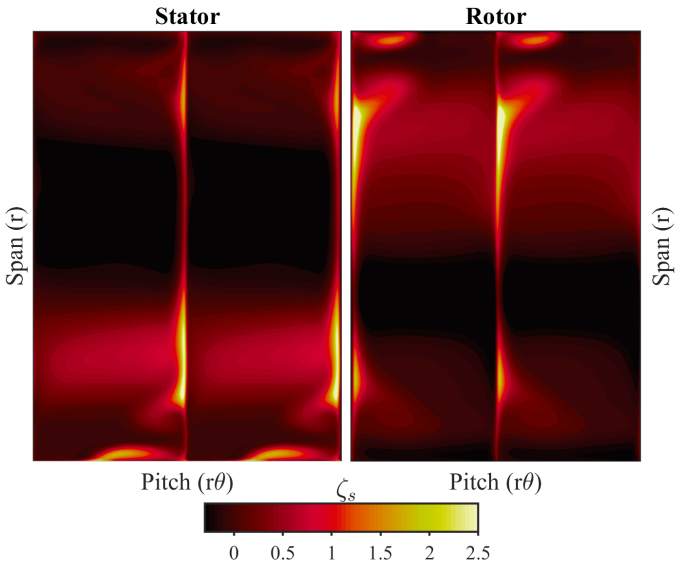

(a) NRT.

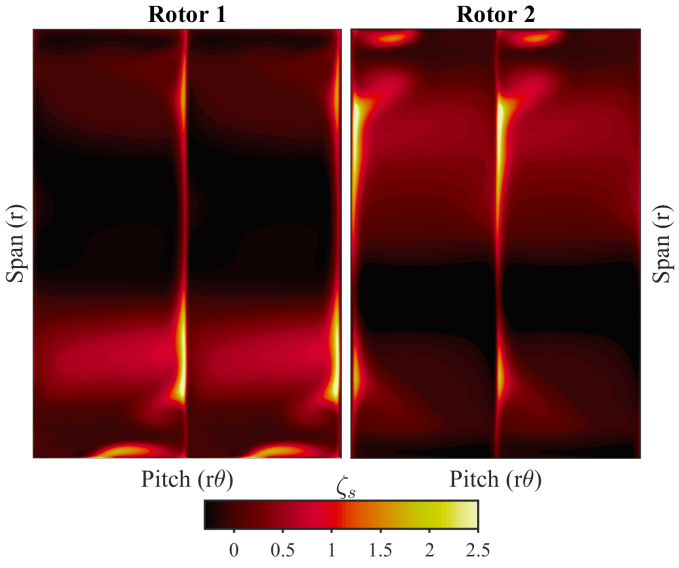

(b) CRT.

FIGURE 7: Contour plots of the local entropic loss coefficient, ζ_s, for a normal and counter-rotating turbine with tip gaps of 5% blade inlet span at $M_{3_{rel}} = 0.4$. Shown at blade exit in the circumferential-radial plane. Each slice is two blade pitches wide.

Copyright © 2019 by ASME

FINITE RADIUS, FINITE SPAN

Design of Numerical Study

A real turbomachine operates at a finite radius, so the effects of radial equilibrium must be considered. A steady flow with no radial velocity is modelled by the simple radial equilibrium equation,

$$\frac{\partial h_0}{\partial r} = T\frac{\partial s}{\partial r} + \frac{1}{2r^2}\frac{\partial \left(rV_\theta\right)^2}{\partial r} + \frac{1}{2}\frac{\partial V_x{}^2}{\partial r}. \tag{13}$$

The implication of Eq. (13) is that all quantities are in the absolute frame of reference, meaning that there is a difference in the velocity distribution radially between NRTs and CRTs due to differences in absolute swirl velocity, resulting in different spanwise blade designs.

In order to maintain a consistent comparison between CRTs and NRTs, the midspan blade section is designed using matching relative parameters, as with the previous sections. The spanwise variation of blade design follows the same vortex distribution in both cases. A free vortex design was chosen, due to its common use and the following properties: free vortex design aims for a uniform axial velocity distribution and a swirl distribution inversely proportional to the radius,

$$\frac{\partial V_x}{\partial r} = 0, \qquad \frac{\partial \left(rV_\theta\right)}{\partial r} = 0. \tag{14}$$

For isentropic models, Eq. (14) results in radially uniform stagnation enthalpy. The radially uniform axial velocity means the maximum velocity through the blade is reduced, resulting in lower profile loss from V^3 losses [26].

To investigate the differences in spanwise blade design between CRTs and NRTs, two different CFD techniques were used. In the first approach, an isentropic, inviscid throughflow solver was used to provide an initial prediction of the differences in performance and the ideal flow field to guide design. The throughflow solver was written for this investigation and designed to model a repeating stage with constant midspan axial velocity through the stage. The solver does this by passing the outlet axial velocity, V_x, and angular momentum, rV_θ, back to the inlet, with the midstage and outlet fixed at a free vortex design, and adjusting the annulus height to fix the axial velocity.

In the second approach, Turbostream was used to acquire fully viscous computational results. This was a two step process. Initially, the model had inviscid slip endwalls which removes secondary flows and avoids designing to cancel endwall overturning. An initial guess was based on the throughflow solver results. During this calculation, the blade metal angles were adjusted iteratively upon convergence to match the relative flow angles to the throughflow predictions. This accounted for the variation of deviation across the blade span. Once the relative flow angles matched those from the throughflow solver, the fully viscous endwalls were included and the metal angles fixed. The output of this simulation provides the final performance results.

The midspan design point used is the same as that given in Table 2 except with a hub-to-tip ratio (HTR) less than 1. This data is used to calculate the appropriate midspan radius, which remains constant throughout the stage. Tip gaps are not included, and the endwalls rotate with the adjacent blade, as with the earlier simulations.

Results

Figure 8 shows the throughflow solver predictions for spanwise variation of local reaction for different values of HTR. The CRT is close to 50% reaction for the entire span whilst the NRT moves away from 50% reaction towards the hub and tip, especially at low values of HTR.

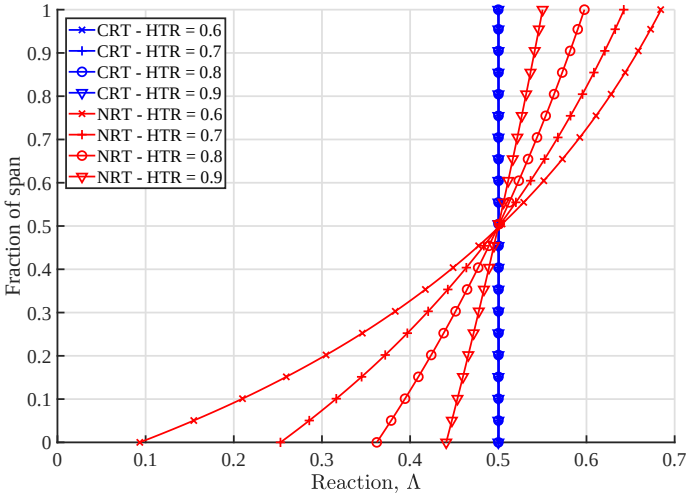

FIGURE 8: Variation of local reaction across the span for different values of hub-to-tip ratio, HTR, calculated using the throughflow solver.

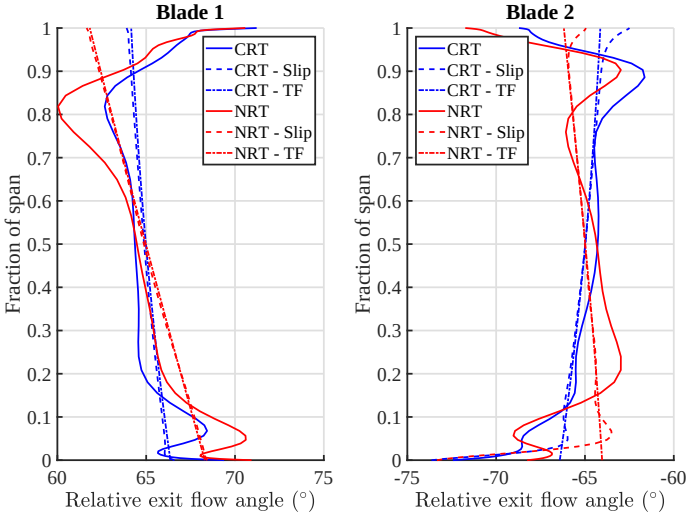

FIGURE 9: Comparison of the final, inviscid slip endwall and throughflow solver calculations of the flow angle relative to the blade at each blade outlet. Slip corresponds to inviscid slip endwalls and TF corresponds to throughflow solver. All results calculated for a hub-to-tip ratio of 0.75.

Before the performance of the two types of turbine is investigated, the agreement between the final flow field produced by the viscous CFD and the design intentions is checked. Figure 9 shows the relative flow angle at blade exit in the three phases of the design process. Overall, there is good agreement between the final viscous calculations and the throughflow predictions. Towards the endwalls, the flow suffers from overturning due to secondary flows and there is around 1° additional deviation at midspan due to endwall blockage. However, the midspan flow of the NRT and CRT still match each other due to the use of relative parameters.

The throughflow solver predicts that CRTs have 50% reaction across the span, even at low HTR, Fig. 8. This implies CRTs could

Copyright © 2019 by ASME

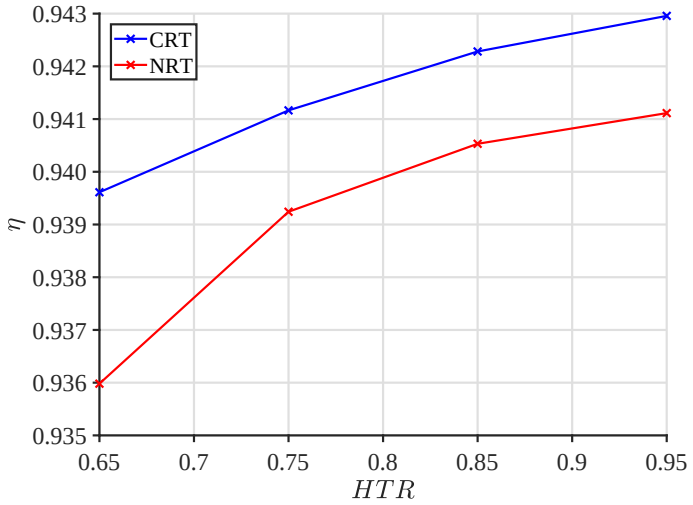

FIGURE 10: Variation of isentropic efficiency, η, against hub-to-tip ratio, HTR, from the viscous CFD calculation.

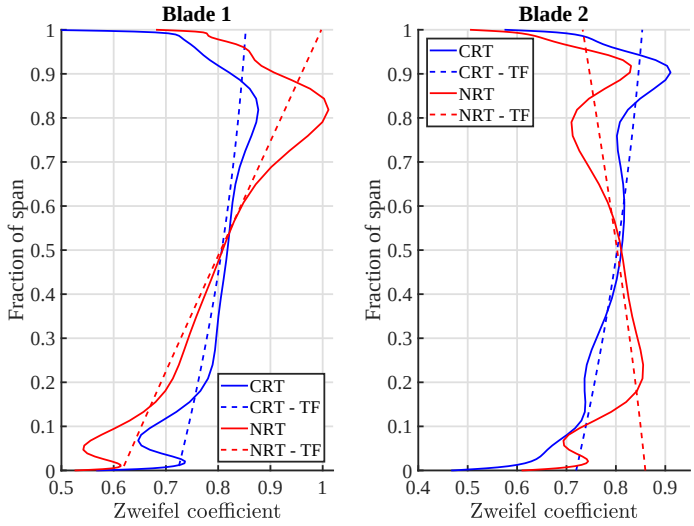

FIGURE 11: Variation of Zweifel coefficient up the span from the final results, compared to those predicted from the throughflow solver, TF, for the two blade rows. Calculated at a hub-to-tip ratio of 0.75.

have an improved performance over NRTs, which is confirmed in Fig. 10. This figure shows an improved efficiency for CRTs compared to NRTs. The improvement in efficiency increases as the HTR decreases, to a value of 0.36% at a HTR of 0.65.

The reasons for the CRT's superior performance become apparent in Figs. 11 and 12. In Fig. 11, the throughflow solver and final viscous CFD calculations show the Zweifel coefficient is higher towards the tip on the first blade and the hub of the second blade for the NRT, when compared to the CRT. This contributes towards higher blade loading in these areas, resulting in increased loss coefficient shown in Fig. 12. The effect of spanwise variation in loading results in increased overall loss for the NRT. At midspan, the two types of turbine have the same performance due to the matched relative parameters.

It has already been shown that CRTs can produce the same power output and efficiency per stage with half the midspan radius when compared to an equivalent NRT, Table 1. However, the

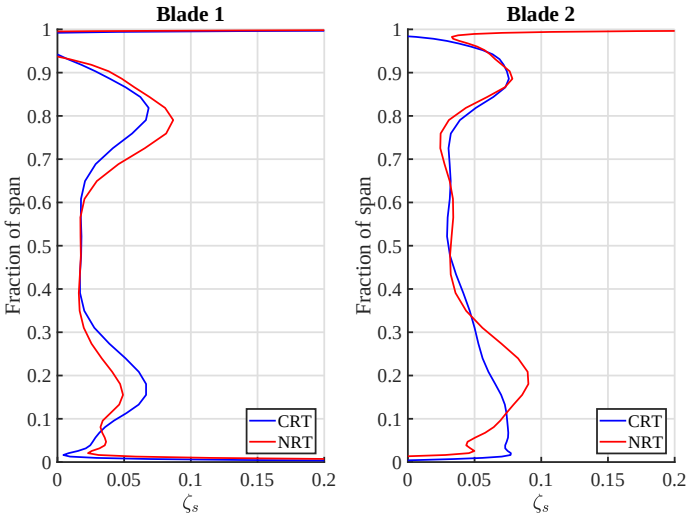

FIGURE 12: Spanwise variation of pitchwise averaged entropic loss coefficient, ζ_s, for the CRT and NRT from the viscous CFD calculation. Calculated at a hub-to-tip ratio of 0.75.

three-dimensional analysis at finite radius now shows that CRTs have a performance advantage at lower hub-to-tip ratios when compared to NRTs. This makes CRTs an attractive option for high power density applications.

COUNTER-ROTATING COMPRESSOR DESIGN

To demonstrate that the advantage of counter-rotation extends to compressors, a study using the isentropic throughflow solver from the turbine study was carried out. Relative parameters were used to define a repeating stage, midspan design for both an NRC and CRC. As with the turbine study, the midspan relative flow coefficient, relative stage loading and reaction were matched between the conventional and counter-rotating machines, resulting in the same midspan relative flow field and performance. These values, along with the aspect ratio and hub-to-tip ratio are given in Table 3. However, the pitch-to-chord ratio is now set by the diffusion factor, DF. A free vortex design Eq. (14) is chosen to define the velocity distributions up the span of the blades, resulting in different radial blade designs due to radial equilibrium Eq. (13).

ϕ_r	0.6	χ_1	$-49.8°$
ψ_r	0.4	χ_2	$-27.5°$
Λ	50%	HTR	0.75
DF	0.45	Re_x	3×10^5
AR	2	$M_{3_{rel}}$	0.4

TABLE 3: Midspan design point data for the compressor study.

Figures 13 and 14 show that the first blade row of the NRC is more twisted than the CRC. The twist is comparable for the second blade row. Figure 15 shows that the NRC has a greater variation

Copyright © 2019 by ASME

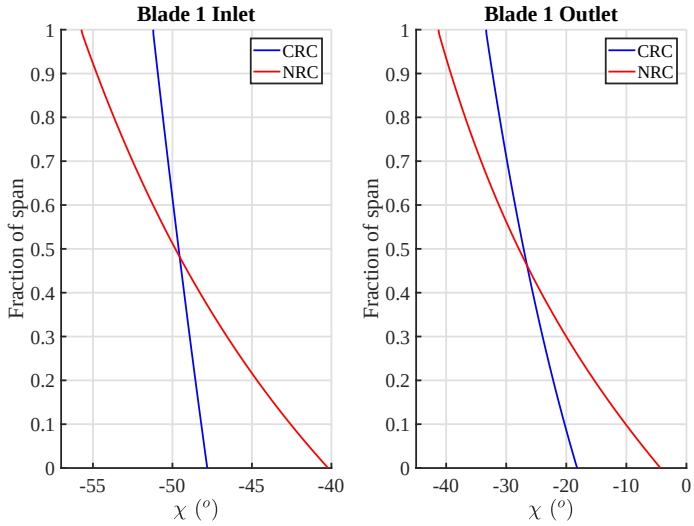

FIGURE 13: Comparison of throughflow solver predictions of metal angles for the first blade row for CRC and NRC.

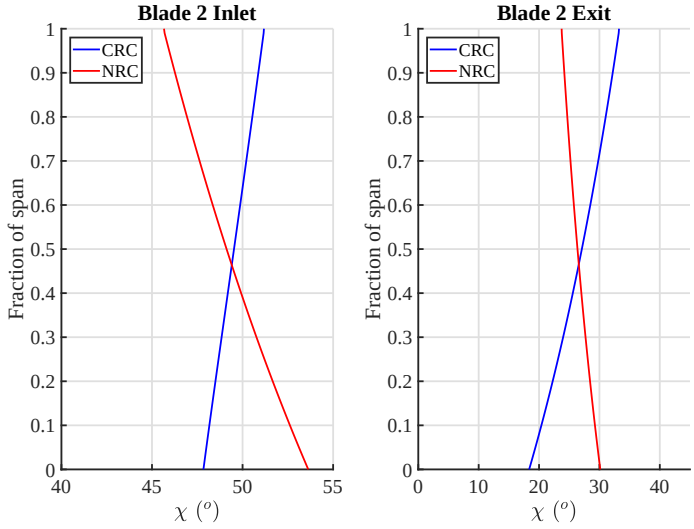

FIGURE 14: Comparison of throughflow solver predictions of metal angles for the second blade row for CRC and NRC.

of diffusion factor up the span, whilst the CRC spanwise diffusion factor distribution is more uniform. For both blade rows, the NRC has a higher peak diffusion factor, meaning the number of blades must increase to maintain the same peak diffusion factor, especially on the second blade row. This will result in part of the NRC span being over-bladed producing more loss compared to the CRC.

CONCLUSIONS

The following conclusions are made from this study:

1. The performance of conventional (normal) rotating turbines (NRTs) and counter-rotating turbines (CRTs) can be compared as part of the same design space by using correctly defined *relative parameters*. A two blade row, counter-rotating stage is the same as a conventional stage when viewed in a reference frame rotating with the *first blade row*. This method ensures the performance of both CRTs and NRTs is matched for the same design parameters. This idea also applies to conventional and counter-rotating compressors.
2. Previous studies have reported improvements in efficiency for counter-rotating turbines. This study shows that this benefit is achieved by moving across the Smith Chart defined by relative parameters to a region of higher efficiency.
3. By matching the relative parameters of an NRT and CRT with the same relative blade speed, both turbines will have the same midspan performance but the CRT can be designed to have either half the angular velocity of the NRT or half the midspan radius, significantly increasing the CRT power density.
4. By matching the relative parameters of an NRT and CRT with the same absolute blade speed the CRT will have four times the power output per two blade stage. The CRT will also have the same performance as an NRT, except for losses associated with doubled relative Mach numbers.
5. It has been shown that, when designed with the same relative parameters and relative inlet conditions, CRTs and NRTs have the same profile losses, secondary flows and tip losses at an infinite radius. These phenomena are not directly effected by counter-rotation.
6. Due to differences in absolute swirl velocity, radial equilibrium drives CRTs and NRTs to different three-dimensional blade designs at finite radius. For low hub-to-tip ratios, CRTs gain a performance advantage over comparable NRTs due to a lower loading variation along the blade span, especially on the first blade row. This effect is also apparent in the comparison of conventional and counter-rotating compressors using isentropic throughflow predictions.

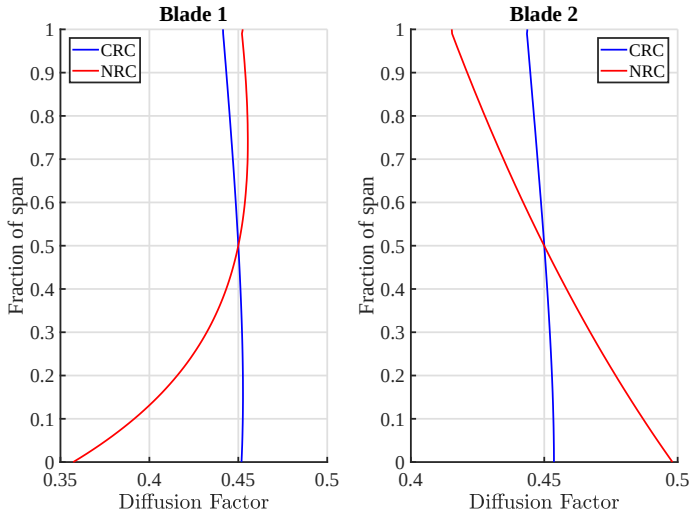

FIGURE 15: Variation of diffusion factor up the span for a CRC and NRC predicted by the throughflow solver.

ACKNOWLEDGEMENTS

The authors are grateful for the support of Reaction Engines Limited during the course of this project, and, in particular, the assistance of Marc Arstall, Osama Lotfi and Philippa Davies.

Copyright © 2019 by ASME

NOMENCLATURE

Abbreviations

CFD	Computational Fluid Dynamics
NRT	Normal (Conventional) Rotating Turbine
CRT	Counter-Rotating Turbine
NRC	Normal (Conventional) Rotating Compressor
CRC	Counter-Rotating Compressor
HTR	Hub-to-Tip Ratio
AR	Aspect Ratio

Symbols

ϕ	Flow coefficient
ψ	Stage loading coefficient
ϕ_r	Relative flow coefficient
ψ_r	Relative stage loading coefficient
Λ	Reaction
r	Radius (m)
r_m	Midspan radius (m)
Ω	Shaft rotational speed ($rads^{-1}$)
U	Blade velocity (ms^{-1})
U_1	Blade velocity of first row (ms^{-1})
U_2	Blade velocity of second row (ms^{-1})
U_f	Reference frame velocity (ms^{-1})
U_r	Relative blade velocity (ms^{-1})
V_x	Axial velocity (ms^{-1})
V_θ	Tangential/swirl velocity (ms^{-1})
h	Specific static enthalpy (Jkg^{-1})
h_0	Specific stagnation enthalpy (Jkg^{-1})
s	Static entropy ($Jkg^{-1}K^{-1}$)
T	Static temperature (K)
T_0	Stagnation temperature (K)
T_{01_r}	Inlet stagnation temperature relative to first blade row (K)
α_{1_r}	Inlet flow angle relative to first blade row ($^\circ$)
α_{2_r}	Midstage flow angle relative to first blade row ($^\circ$)
α_{3_r}	Stage exit flow angle relative to the first blade row ($^\circ$)
χ_1	Leading edge blade metal angle ($^\circ$)
χ_2	Trailing edge blade metal angle ($^\circ$)
δ	Deviation ($^\circ$)
C_x	Axial chord (m)
γ	Ratio of heat capacities
R	Ideal gas constant ($Jkg^{-1}K^{-1}$)
c_p	Specific heat capacity ($Jkg^{-1}K^{-1}$)
$M_{3_{rel}}$	Exit Mach number relative to second blade row
Re_x	Axial inlet Reynolds number
Z	Zweifel coefficient
DF	Diffusion factor
η	Isentropic efficiency
ζ_s	Entropic loss coefficient

REFERENCES

[1] Hooker, S., 1991. *Not Much of an Engineer, An Autobiography*. The Crowood Press Ltd., Marlborough, UK.

[2] Wintucky, W. T., and Stewart, W. L., 1958. "Analysis of Two-Stage Counterrotating Turbine Efficiencies in Terms of Work and Speed Requirements". In *NACA Research Memorandum*. NACA. RM E57L05.

[3] Cai, R., Wu, W., and Fang, G., 1990. "Basic Analysis of Counter-Rotating Turbines". In Gas Turbine and Aeroengine Congress and Exposition, ASME. 90-GT-108.

[4] Reaction Engines Ltd. SABRE. Online, `https://www.reactionengines.co.uk/sabre-engine/`. Last Accessed: July 2018.

[5] Paniagua, G., Szokol, S., Kato, H., Manzini, G., and Varvill, R., 2008. "Contrarotating Turbine Aerodesign for an Advanced Hypersonic Propulsion System". *Journal of Propulsion and Power,* ***24***(6), pp. 1269–1277.

[6] Paniagua, G., Lavagnoli, S., Verstraete, T., Mahmoudi, W., and Benamara, T., 2011. "Aero-Design of Transonic LH2 and LOX Contra Rotating Turbopumps in an Expander Rocket Engine". *International Journal of Numerical Methods for Heat and Fluid Flow,* ***23***(4), pp. 575–587.

[7] Pempie, P., and Ruet, L., 2003. "Counter-Rotating Turbine Designed for Turbopump Rocket Engine". In Joint Propulsion Conference and Exhibit, AIAA/ASME/SAE/ASEE. AIAA 2003-4768.

[8] Alexiou, A., Roumeliotis, I., Aretakis, N., Tsalavoutas, A., and Mathioudakis, K., 2012. "Modelling Contra-Rotating Turbomachinery Components for Engine Performance Simulations: The Geared Turbofan with Contra-Rotating Core Case". In Turbo Expo 2012, ASME. GT2012-69433.

[9] Schimming, P., 2003. "Counter Rotating Fans - An Aircraft Propulsion for the Future?". *Journal of Thermal Science,* ***12***(2), pp. 97–103.

[10] Bellocq, P., Garmendia, I., Legrand, J., and Sethi, V., 2016. "Preliminary Design and Performance of Counter Rotating Turbines for Open Rotors - Part I: 1-D Methodology". In Turbo Expo 2016: Turbomachinery Technical Conference and Exposition, ASME. GT2016-57918.

[11] Bellocq, P., Garmendia, I., Legrand, J., and Sethi, V., 2016. "Preliminary Design and Performance of Counter Rotating Turbines for Open Rotors - Part II: 0-D Methodology and Case Study for a 160 PAX Aircraft". In Turbo Expo 2016: Turbomachinery Technical Conference and Exposition, ASME. GT2016-57921.

[12] Murakami, T., and Kanemoto, T., 2013. "Counter-Rotating Type Pump-Turbine Unit Cooperating with Wind Power Unit". *Journal of Thermal Science,* ***22***(1), pp. 7–12.

[13] Kanemoto, T., Kasahara, R., Honda, H., Miyaji, T., and Kim, J., 2013. "Counter-Rotating Type Pump-Turbine Unit Stabilizing Momentarily Fluctuating Power from Renewable Energy Sources". In International Mechanical Engineering Congress and Exposition, ASME. IMECE2013-66000.

[14] Zhao, W., Xu, J., and Wu, B., 2014. "Aerodynamic Design and Analysis of a Multistage Vaneless Counter-Rotating Turbine". In Turbo Expo 2014: Turbine Technical Conference and Exposition, ASME. GT2014-26335.

[15] Wei, S., and Kun, Z., 2015. "Design for High MA Number Counter Rotating Turbine Blades". In Turbo Expo 2015: Turbine Technical Conference and Exposition, ASME. GT2015-43374.

[16] Zhou, K., Liu, H., Zou, Z., and Wang, L., 2014. "Aerodynamic Design of Three-Stage Vaneless Counter-Rotating Turbine". *Journal of Aerospace Power,* ***29***(7), pp. 1667–1679.

Copyright © 2019 by ASME

[17] Louis, J. F., 1985. "Axial Flow Contra-Rotating Turbines". In Gas Turbine Conference and Exhibit, ASME. 85-GT-218.
[18] Sharma, P. B., and Adekoya, A., 1996. "A Review of Recent Research on Contra-Rotating Axial Flow Compressor Stage". In International Gas Turbine and Aeroengine Congress and Exposition, ASME. 96-GT-254.
[19] Sharma, P. B., Jain, Y. P., and Pundhir, D. S., 1988. "A Study of Some Factors Affecting the Performance of a Contra-Rotating Axial Compressor Stage". *Proceedings of the Institute of Mechanical Engineers,* ***202***(A1), pp. 15–21.
[20] Gao, L., Li, X., Xie, J., and Liu, B., 2012. "The Effect of Speed Ratio on the First Rotating Stall Stage in Contra-Rotating Compressor". In Turbo Expo 2012, ASME. GT2012-68802.
[21] Kerrebrock, J. L., Epstein, A. H., Merchant, A. A., Guenette, G. R., Parker, D., Onnee, J., Neumayer, F., Adamczyk, J. J., and Shabbir, A., 2008. "Design and Test of an Aspirated Counter-Rotating Fan". *ASME Journal of Turbomachinery,* ***130***(2).
[22] Smith, S. F., 1965. "A Simple Correlation of Turbine Efficiency". *Journal of the Royal Aeronautical Society,* ***69***, pp. 467–470.
[23] Craig, H. R. M., and Cox, H. J. A., 1971. "Performance Estimation of Axial Flow Turbines". *Proceedings of the Institute of Mechanical Engineers,* ***185***, pp. 407–424.
[24] Denton, J. D., 2017. "Multall - An Open Source, Computational Fluid Dynamics Based, Turbomachinery Design System". *ASME Journal of Turbomachinery,* ***139***(12).
[25] Brandvik, T., and Pullan, G., 2011. "An Accelerated 3D Navier-Stokes Solver for Flows in Turbomachines". *ASME Journal of Turbomachinery,* ***133***(2).
[26] Denton, J. D., 1993. "Loss Mechnisams in Turbomachines". *ASME Journal of Turbomachinery,* ***115***(4), pp. 621–656.

APPENDIX - CFD CONFIGURATION

All CFD calculations were performed using Turbostream [25]. Turbostream is a three-dimensional Navier-Stokes solver primarily designed for turbomachinery calculations. It can handle multiple blocks of structured grids which are patched together to model the various connecting boundary conditions. The solver uses a finite volume method with a Spalart-Allmaras turbulence model.

The domain of the two-dimensional mesh around each blade extends to half an axial chord upstream and downstream of the blade. The mesh consists of 168 nodes axially (100 along the blade, 40 upstream and 30 downstream) and 40 pitchwise. The entire domain of each calculation consists of two blades to model a single stage, with a mixing plane used to connect the domains of the individual blades. All calculations are steady.

To model the repeating stage for the two-dimensional blade sections, the pitchwise distributions of stagnation temperature, stagnation pressure and flow angle at the outlet plane are passed back to the inlet, once the solution has converged. To account for changes through the stage, the outlet stagnation temperature and stagnation pressure distributions have the difference in the mean between inlet and outlet restored when passed back to the inlet. These conditions are implemented to produce the correct flow angles for the repeating stage model, and to model boundary layer build up on the endwall surfaces. Convergence is achieved after 6 iterations of this process.

For the "cascade" calculation, the mesh for each blade is kept the same in the axial-pitchwise plane, and 40 spanwise nodes are added. The whole domain of each calculation is still a two blade repeating stage. In order to keep the axial velocity constant, and maintain a repeating stage condition, the annulus height increases along the stage. This is achieved based on an initial guess from isentropic conditions, followed by iterative annulus height adjustments within the CFD calculations. This area change is implemented over the chord of each blade, with a constant area being maintained between the trailing and leading edge of adjacent blades, Fig. 5.

Due to the difference in inlet and outlet areas, the method of passing the conditions at the outlet plane back to the inlet for a repeating stage was updated. The pitchwise averaged flow angles, stagnation temperature and stagnation pressure (the latter two adjusted for changes in the mean value) are passed from each percentage distance up the span at outlet to the same percentage at inlet. This process is done iteratively, along with updating the annulus height. Convergence is achieved within 10 iterations of this process. When tip gaps are added, the mesh is extended to have 79 nodes in the spanwise direction (60 along the blade and 20 in the gap) and 60 nodes pitchwise. The gaps cover 5% of the blade span.

For the finite radius, finite span calculations, the domain remains as two blades, but the mesh is increased to 168 nodes axially, 60 nodes pitchwise and 60 nodes spanwise. A repeating stage is only applied to the final, fully viscous calculation.

Copyright © 2019 by ASME